ACS OMEGA

http://pubs.acs.org/journal/acsodf

Article

Fundamental Properties of Hydrogen-Functionalized GaSe Monolayer

Thi My Duyen Huynh,* Thi Dieu Hien Nguyen, and Ming-Fa Lin*

Cite This: *ACS Omega* 2022, 7, 34868−34876

Read Online

ACCESS | Metrics & More | Article Recommendations | Supporting Information

ABSTRACT: Functionalization reveals potential opportunities for modifying essential properties and designing materials due to the strong interaction between functionalized atoms and the surface. Among them, hydrogenation possesses such a way to control electronic and optical characteristics. In this paper, the stability and transformed electronic, optical properties of H-functionalized GaSe in two cases (single and double sites) were reported that exhibit the effects of hydrogen functionalization via first-principles calculations. Formation energies suggest that H-functionalized GaSe systems are stable for construction. H-GaSe and 2H-GaSe display distinct properties based on the functionalized way (single- or double-site functionalization). Accordingly, H-GaSe is metallic, while 2H-GaSe belongs to a semiconductor. The magnetic configuration with ferro- and anti-ferromagnetic could be found in H- and 2H-functionalized cases through spin distribution, respectively. Especially, the chemical hybridized bonds of Se−H, Ga−Se, and Ga−Ga corresponding to s-sp^3 and sp^3-sp^3 bondings, respectively, are clearly verified in the orbital-projected density of states and charge density. The optical properties of 2H-GaSe could provide the main characteristics of a semiconductor, which is the limited range of transparency by electronic absorption at short and long wavelengths. Moreover, increasing the number of GaSe segments (L) could change the band gap leading to application in the band gap engineering of the 2H-GaSe systems. Thus, hydrogen functionalization could provide the possible manner for adjusting and controlling features of GaSe, promising for the development of electronic devices and applications.

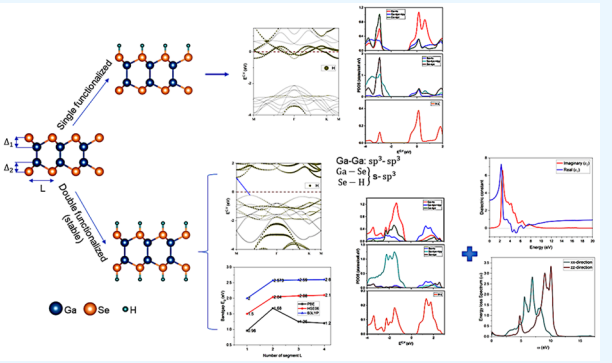

INTRODUCTION

Two-dimensional (2D) materials have covered a wide range of specifications[1] and applications[1,2] due to their various features in many fields such as electronics, optoelectronics, conductivity, and energy storage.[3−8] Because of success in graphene and graphene-based investigations,[2,9−15] 2D materials, particularly honeycomb structures, have generally gained more and more attention for designing next-generation devices. In 2D materials, the physical and chemical properties strongly and consistently depend on geometric properties, leading to the necessity and significance of solving structural problems. The surface process including doping, intercalation, or functionalization is one of the main issues of structural problems to mark their signature in applications. Because of the limitations of pristine 2D materials in industrial applicability, this process provides an efficient method for modifying original material properties that have been developed in modern applications.[16] Hence, addressing the surface process becomes a key to determine the potential of the material.

Surface processing of 2D materials has various strategies including doping,[17−19] adsorption,[16,20] substitution,[17] intercalation,[21,22] and functionalization[3,23−26] based on their efficient interacting environment compared to bulk counterparts. Among them, functionalization can create a chemical environment for adjusting properties,[27] which supports fabrication[28] or material growth.[29] Even though the functionalized nature remains unclear, this process has predicted the existence of remarkable effects on a surface reaction for plenty of fields. Functionalization in graphene and related graphene systems indicate high performance in the efficient storage capacity,[3,4,24,30] the hydrogen evolution reaction (HER),[20,26,31−35] growth mechanism,[12] and photoelectrochemical generation.[28] Furthermore, functionalization can tune the electronic and mechanical properties[32,36] of certain 2D materials resulting in tellurene structures[37] and MoS_2,[38] respectively. Oxidation and hydrogenation are the two common parameters of functionalization in 2D materials,[3,23−26,29,33−35,37] in which the structure is functionalized by oxygen and hydrogen atoms, respectively. They all also

Received: June 1, 2022
Accepted: August 25, 2022
Published: September 22, 2022

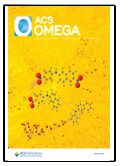

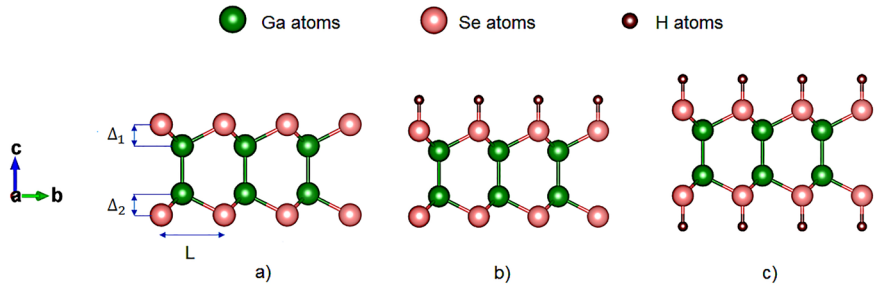

Figure 1. Structural optimization of (a) pristine monolayer, (b) single, and (c) double hydrogen functionalization GaSe from the side view with (yz) plane.

Table 1. Structural Parameters of Pristine and H-Functionalized GaSe in the Single and Double Side

				chemical bond (Å)			buckling Δ (Å)	
system	E_f (eV)	magnetic moment	lattice constant (Å)	Ga−Ga	Ga−Se	Se−H	(1)	(2)
pristine		0	3.85	2.49	2.48		1.115	
H-GaSe	−1.38	−0.01	4.14	2.65	2.7	1.52	1.24	0.96
2H-GaSe	−3.92	0	4.24	3.84	2.8	1.49	1.37	1.36

provide useful information concerning the mechanical response[33,38] in graphene, germanene, MoS_2, and Ti_3C MXene.

On the other hand, with the development of graphene and graphene-based materials,[39−41] the metal chalcogenides group has gained rapidly growing interest.[7,42−47] The metal monochalcogenides labeled MX (M: metal; X: chalcogen atoms)[48−50] are one class of this group that has been synthesized and analyzed in both experimental and theoretical studies.[44,46,50−54] As a typical member of the MX group, GaSe is an emergent candidate due to its excellent performance in nonlinear optics[55] and the generation of electromagnetic waves. To enhance its optical properties, various elements including S, Te, Ag, and Al have been doped on GaSe crystal[56−59] suggesting the further optimum growth technique. Meanwhile, the transformation between a trivial and nontrivial topological insulator of GaSe has been found after functionalizing with oxygen,[60] forming the quantum Hall effect. This motivates one to turn to hydrogen functionalization on GaSe for new opportunities in documented research and applications. Although the natural interaction between hydrogen and a surface through a functionalized structure has been a subject of debate,[4,30] hydrogenation possesses promise and is a potential manner for the design and growth of materials.[3,12,20,24,31,36,38] In addition, hydrogen functionalization has been absent in surface processes of GaSe up to now. Therefore, unique and critical features such as the transformation of electronic properties, band gap engineering, and essential optical properties will be expected to be revealed in the hydrogenation of GaSe. In this work, the stability and electronic and optical properties of H-functionalized GaSe are systematically investigated by implementing first-principles calculations for clarifying the interaction between hydrogen atoms and GaSe surface. As a result, the interacting bondings of hydrogen and the surface as well as the inside interaction of the functionalized system are consistently described through a multiorbital hybridization concept, demonstrating diverse band energy spectra, density of state, and optical properties. Accordingly, frequency dependence of the dielectric function is able to define important optical properties as fundamental for future discussion on exciton effects on the system.

METHODOLOGY

First-principles calculations implemented in the VASP package[61] were performed for investigating geometric, electronic, and optical properties of hydrogenation GaSe. A vacuum of 15 Å was set to avoid the interaction between neighboring slabs in the structure. For electron exchange-correlation interactions, the generalized gradient approximation (GGA)[62] of the Perdew−Burke−Ernzerhof functional (PBE)[63] was applied with the cutoff energy of 500 eV. Moreover, the hybrid functional Heyd-Scuseria-Ernzerhof (HSE06)[64,65] and Becke, three-parameter, Lee−Yang−Parr (B3LYP)[66] were implemented for more accurate band gap calculations and making a comparison. The values of 10^{-5} eV and 0.001 eV/ Å were set for the criteria of energy and force, respectively. The k-points of 15 × 15 × 1 in gamma symmetry and high-symmetric Γ-centered grid Brillouin zone were sampled for structural optimization and band energy calculations, respectively.

RESULTS AND DISCUSSION

Monolayer GaSe (Figure 1a) presents a stacked Se−Ga−Ga−Se slab as a member of metal monochalcogenides MX,[48,49] which are formed in a hexagonal structure with the space group of $P6m2$.[55,67] The hydrogen-functionalized GaSe was constructed in single and double sites in which the hydrogen atoms were directly doped on the top and both sites of selenium atoms as shown in Figure 1b,c, respectively. In this figure, the optimized structures of pristine and hydrogen-functionalized GaSe were illustrated in single and double sites, namely, H-GaSe and 2H-GaSe, respectively, from the side view. The formation energy (E_f) was considered to confirm the functionalized favorability of GaSe monolayer according to eq 1

$$E_f = E_{sys} - \left(E_{GaSe} + \frac{\mu_{Se} + \mu_H}{2}\right) \quad (1)$$

where E_{sys} and E_{GaSe} are the total energy of the functionalized and pristine systems, respectively; μ_{Se} and μ_H are, respectively, the chemical potential of selenium in their bulk phases. Number 2 is used to calculate the double-site functionalization. The formation energies indicate that 2H-GaSe is more stable than H-GaSe based on the smaller value (−3.92 eV) as

https://doi.org/10.1021/acsomega.2c03198
ACS Omega 2022, 7, 34868−34876

mentioned in Table 1. Furthermore, this value is close to the formation energies of some stable 2D materials, for example, graphene[68,69] and MoS_2.[70] This predicts the possibility of constructing double-site H-functionalized GaSe for practical applications.

The structural parameters shown in Table 1 describe the main structural features of H-functionalized GaSe. Functionalization could enlarge the lattice constant from 3.85 to 4.12 and 4.24 Å in single and double types, respectively, leading to increases in the Ga−Ga and Ga−Se bond lengths compared to those of the pristine case as listed in this table. This change might come from the interaction between H and a surface as well as sharing of Se and H charges. A similar feature has been also found in O-functionalized GaSe.[60] Moreover, H-functionalized configurations form two different bucklings, labeled Δ_1 and Δ_2, while identical ones appear in the pristine case as described in Figure 1a and Table 1. 2H-GaSe exhibits a fixed configuration in H-functionalized sites with selenium atoms indicating the larger bond length of the Ga−Ga bond and two buckling values compared to that of the H-GaSe case. Contrarily, the without a H-functionalized site, H-GaSe is more flexible because of the remarkable larger buckling Δ_1 that might cause the gapless behavior in the electronic properties. These two cases demonstrate the essential effect of hydrogen functionalization in the 2D structure of GaSe.

GaSe monolayer exhibits a semiconducting configuration with a middle gap of 2.665 eV calculated with the HSE06 hybrid functional as listed in Table 2. The hydrogen atoms in single-site functionalization reveal the effect of the GaSe monolayer resulting in a gapless structure. However, the double-site H-functionalized case remains the semiconducting configuration with the band gap of 2.08 eV (Table 2). Thus, a functionalized method in a single or double site suggests a way to manipulate the band gap, which could become one of the factors for band gap engineering. Moreover, band gap dependence could be realized in various manners related to structural modifications. In fact, the band gap influence of the double-functionalized system could be considered due to varying the number of GaSe segments (L) in a unit cell as described in Figure 1a and Table 2. In this table, band gaps with changing L were calculated by implementing PBE and hybrid functional HSE06, B3LYP to get accurate band gap values and make a comparison among them. Although there exists a difference of band gap between these two hybrid functional calculations, the trend in the band gap change is the same as that of increasing L. Accordingly, the dramatic change of band gap is found when going from the L = 1 to L = 2 system for all applied functionals; for example, the band gap increases from 1.5 to 2.04 eV by HSE06 functional calculations. From the L = 2 case, the slight enhancement is shown following the increase of the L parameter. Thus, a double-functionalized structure considering the change of value L of segment GaSe could control the band gap suggesting a potential method for the design and construction of this material.

Table 2. Band Gap Engineering (Eg, eV) Varying the Number of Segment L per Unit Cell in the 2H-GaSe System with PBE, HSE06, and B3LYP Functional for Band Gap Calculations

	2H-GaSe				
functional	L = 1	L = 2	L = 3	L = 4	pristine
PBE	0.96	1.68	1.25	1.2	1.8
HSE06	1.5	2.04	2.08	2.1	2.665
B3LYP	2.0	2.573	2.59	2.6	2.96

Even if the band gap depends on the implemented functional as mentioned above, the band energy spectra with main features related to dispersions remain for all cases of functionals. Thus, band energy structures from PBE calculations are presented in Figure 2. In this figure, the distinct properties between pristine and functionalized cases along the high-symmetry path of M-Γ-K-M in the first Brillouin zone (BZ) of hexagonal lattice are accordingly analyzed. The effects of functionalization are indicated in the energy band with many sub-bands due to the increasing number of atoms and orbitals after functionalization. The main features of monolayer GaSe in Figure 2a are further explained in Figure S1 of the Supporting Information. In addition, the type of H-functionalized system exhibits different characteristics of atomic doping as a comparison of single- and double-site functionalization (Figure 2b,c). In Figure 2b, H-GaSe shows the overlap between conduction and valence bands corresponding to a gapless structure. The sombrero hat dispersion is formed at the Γ point and might cause the arising of a van Hove singularity (vHs) in the band-edge state.[71] Moreover, a spacing appears in the range of (−2, −0.5) eV depending on the two asymmetric structural sites. 2H-GaSe (Figure 2c) belongs to a narrow-gap semiconductor that remains the indirect band gap feature from

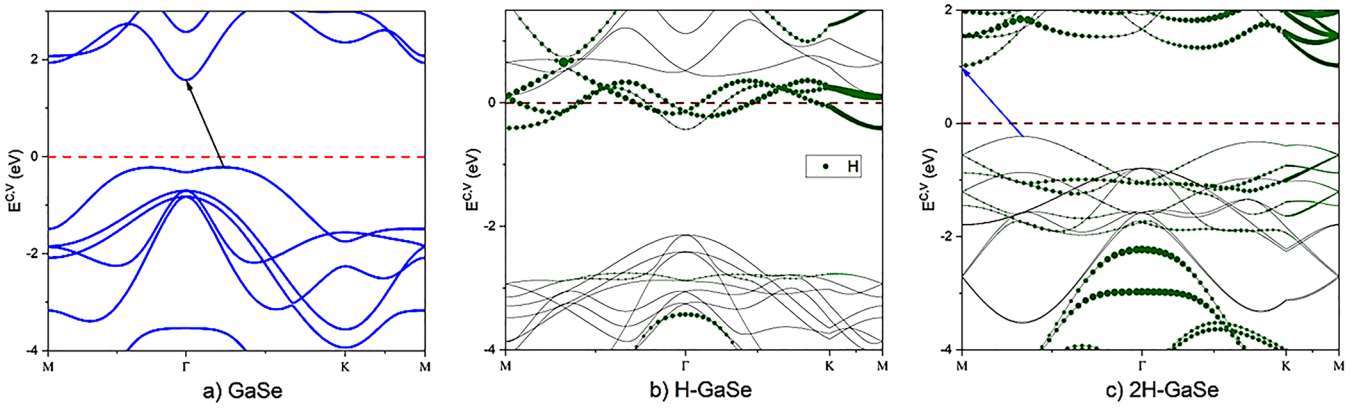

Figure 2. Band energy structures of (a) pristine GaSe and (b) single and (c) double side H-functionalized GaSe with L = 3 and considering hydrogen atom dominance. The green circles represent hydrogen atoms for illustrating its contributions to the band structure.

https://doi.org/10.1021/acsomega.2c03198
ACS Omega 2022, 7, 34868−34876

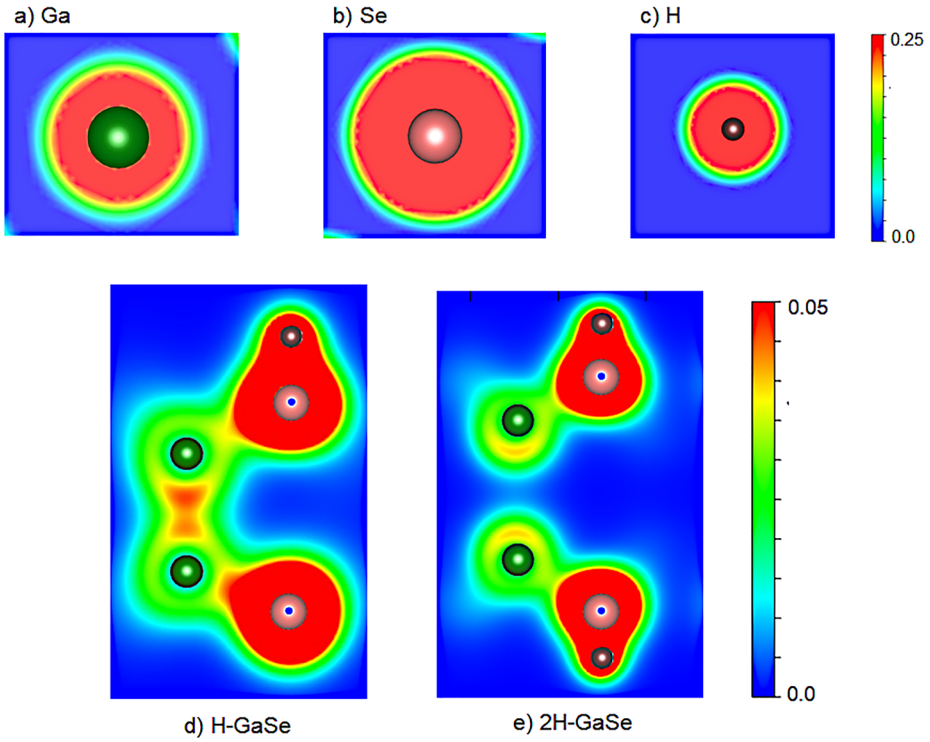

Figure 3. Charge density of isolated atoms (a) Ga, (b) Se, (c) H and H-functionalized GaSe in (d) single and (e) double sites, respectively.

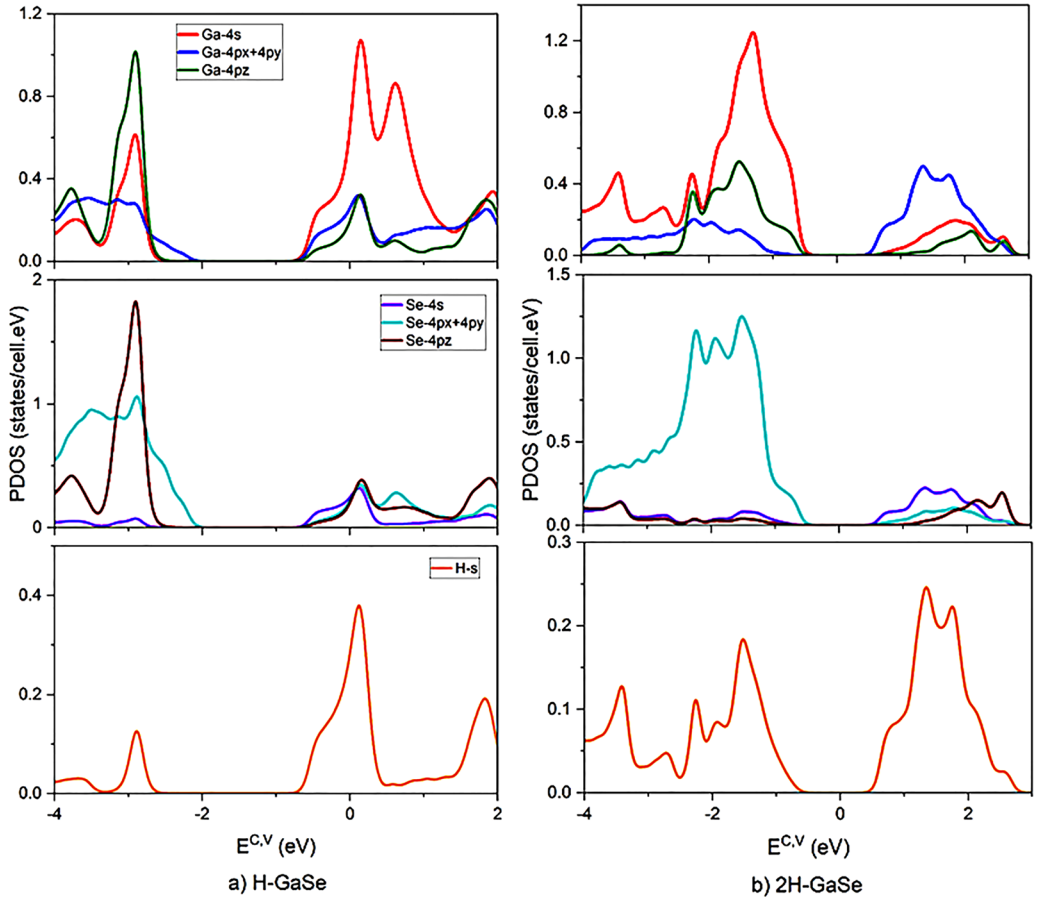

Figure 4. Orbital PDOS of (a) single and (b) double H-functionalized GaSe.

the pristine case indicated in the asymmetry of occupied valence and unoccupied conduction bands about the Fermi level. However, the direction of the VBM-CBM (valence band maximum-conduction band minimum) is transformed in

https://doi.org/10.1021/acsomega.2c03198
ACS Omega 2022, 7, 34868−34876

which the band gap shifts from the M to the point between the M and Γ points while the CBM locates at the Γ point in GaSe monolayer (Figure 2a). Furthermore, strong dispersion is demonstrated in various inverted bands. The parabolic dispersions in the valence band could illustrate that the occupation probability for all states below and above the Fermi level are approximately 1 and free, respectively. Especially, partial flat bands found in the energy range from −3.0 to −1.0 around the Γ point display the orbital interactions in which the electron effective mass should be large.[72] Crossing also appears in the whole range in valence and conduction bands due to the compatibility relations between geometry and eigenstates at the symmetry k-points in the BZ. With regard to atom dominance, hydrogen functionalization demonstrates a strong influence in atomic contribution (green circles) to the system. Based on the main contribution of H atoms near the Fermi level, the band gap of H-GaSe is affected leading to the overlap between conduction and valence bands. In contrast, H atoms reveal strong dominance in the conduction band of 2H-GaSe leading to the open band gap in the band energy spectrum. Hence, H-functionalized GaSe could create remarkable conversion in the band energy structures, which would be promising for material design and applications.

The charge density could provide more information about the type and strength of chemical bonding shown in Figure 3 considering both isolated atoms and compound charge. Isolated atomic charges of all Ga, Se, and H atoms display a spherical-like shape (Figure 3a−c), while those of H-functionalized cases reveal overlap regions of active atoms (Figure 3d,e), indicating chemical bonding of Ga−Ga, Ga−Se, and Se−H. Going from H-GaSe to 2H-GaSe, the overlap between two Ga atoms in a Ga−Ga bond approximately becomes misty corresponding to the increase of Ga−Ga bond length. A similar feature is found in the bond of Ga−Se. These changes might come from the strong effect of two sites of hydrogen functionalization and the contribution of s, p_x, p_y, and p_z orbitals to Ga−Se bonds, respectively. In Se−H bonds, red regions between the H and Se atoms indicate the contribution of s orbitals, while yellow-green regions relate to the p_x, p_y, and p_z orbitals of these two atoms. In the system, H and Ga, Se atoms, respectively, provide s and 4s, $4p_x$, $4p_y$, $4p_z$ active orbitals for H−Se and Ga−Ga, Ga−Se bondings that could determine their chemical bonds for a thorough understanding of the essential properties of hydrogenation structures. To further clarify the essential electronic properties of H-functionalized GaSe in two cases, the orbital projected density of states (PDOS) is considered in Figure 4. The peaks around the Fermi level illustrate the asymmetry of occupied valence and unoccupied conduction bands. In Figure 4a, the strong sp^3 bonding is indicated in the coexisting dominance of s and p orbitals corresponding to (4s, $4p_x$, $4p_y$, $4p_z$)-(4s, $4p_x$, $4p_y$, $4p_z$) of the Ga−Se bond. The sp^3 bonding is also revealed in 2H-GaSe due to the strong dominance of (4s, $4p_x$, $4p_y$, $4p_z$) of Se and Ga atoms, respectively, as shown in Figure 4b. The small but significant contribution of H-s orbitals to form s-sp^3 bondings of H−Se bonds is shown in both cases. Even though both H-GaSe and 2H-GaSe exhibit sp^3 bondings, the orbital contribution is remarkably different, which is caused by the effect of hydrogen atoms based on the functionalized way. These findings additionally indicate the influence of hydrogen atoms on a GaSe monolayer depending on the type of functionalization. Besides, hydrogen-functionalized GaSe displays distinct magnetic behavior corresponding to H-doped single and double sites, resulting in spin density distribution (Figure 5). In Figure 5a, the negative regions with light blue

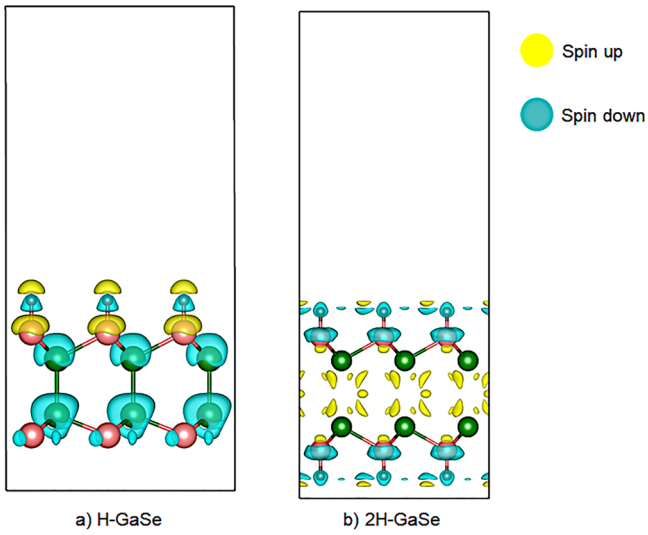

Figure 5. Spin distribution of (a) H-GaSe and (b) 2H-GaSe. Positive and negative values corresponding to spin up and spin down, respectively, are reported in yellow and light blue produced using VESTA.

are extended due to Ga−Se bondings, and the interaction between hydrogen and the surface induce the spin-up configurations colored in yellow. This causes the negative value of magnetic moment as shown in Table 1, leading to a ferromagnetic configuration in this system, while an antiferromagnetic spin distribution occurs across two parallel edges as shown in Figure 5b with zero magnetic moment (see Table 1). The spin-up and spin-down environments lead to the spin splitting indicated in edge and center-initiated spin distributions. Thus, hydrogen-functionalized GaSe could manipulate the magnetic configuration depending on the functionalized manner.

To determine the optical properties of H-functionalized GaSe, related factors including dielectric function, reflectance, refractivity, adsorption, and energy loss spectrum are examined, as shown in Figure 6 and Figure S2. In Figure 6, the optical properties of 2H-GaSe are presented with these main features. The similar characteristics of H-GaSe could be found in Figure S2 of the Supporting Information. The two parts of the dielectric function are described in Figure 6a with a remarkably strong peak (the indicated black arrow) and some weak peaks also mentioned in Table 3 in both real (ε_1) and imaginary (ε_2) parts, colored in violet and red curves. The corresponding relation between these two parts is illustrated via the Kramers−Kronig relationships,[73] which is explained in related formulas (see Supporting Information) and interband transitions in Table 3 and Figure 7. The ultraviolet absorption of 2H-GaSe is caused by these transitions related to its band structure. The absorption spectrum indicates that the system starts to absorb photons in the ultraviolet regions at 2 eV as shown in Figure 6b. The *zz* direction exhibits stronger adsorption in the energy range (4, 10) eV compared to the *xx*/*yy* direction. Besides, the valence excitation region extends up to 7.5 eV, which determines the lowest limit of the conduction band and the upper valence band. The real part behaves mainly as a classical oscillator in which it vanishes in an energy range

https://doi.org/10.1021/acsomega.2c03198
ACS Omega 2022, 7, 34868−34876

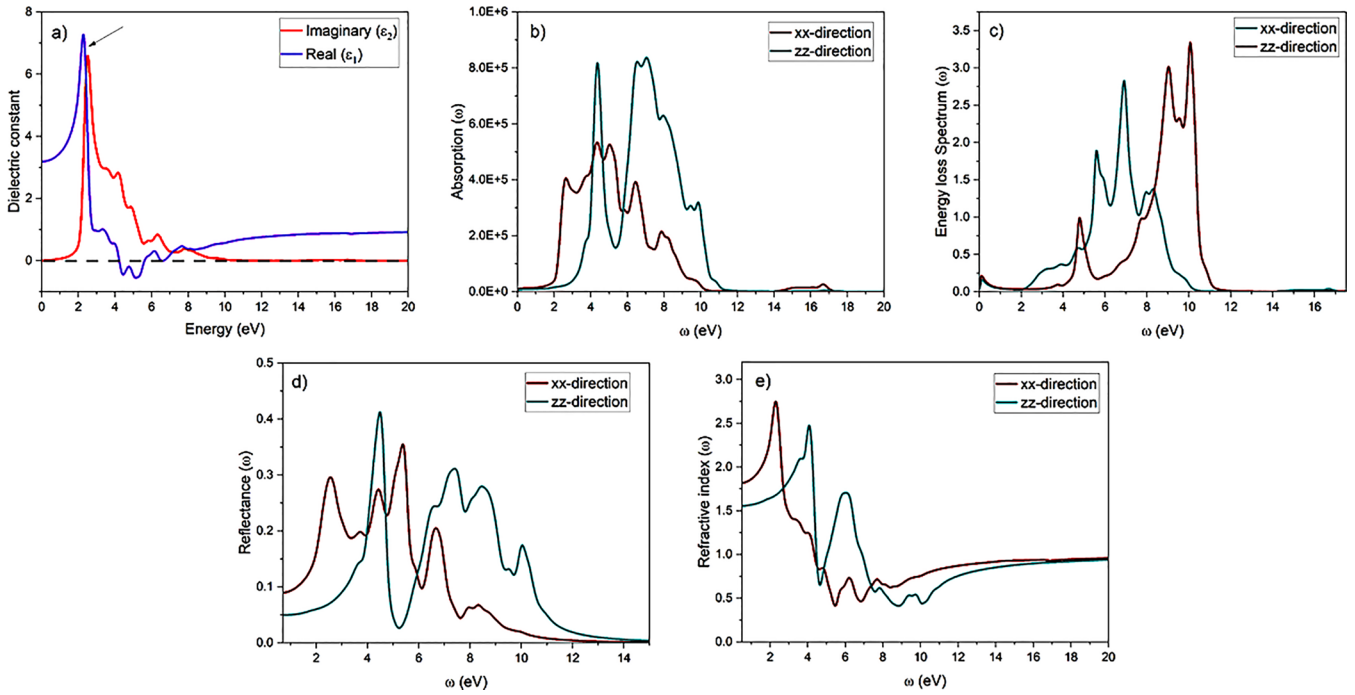

Figure 6. Optical properties of 2H-GaSe through (a) dielectric constant, (b) reflectance, (c) refraction, (d) adsorption coefficient, and (e) energy loss spectrum analysis.

Table 3. Peak Position (eV) of Imaginary Parts and Interband Transition for 2H-GaSe in the Range of (0, 8) eV

peak order	imaginary part	interband transition
1	2.5	M → Γ
2	4.17	M → Γ
3	4.86	Γ → K
4	5.84	Γ → K
5	6.32	Γ → K
6	7.2	M → Γ

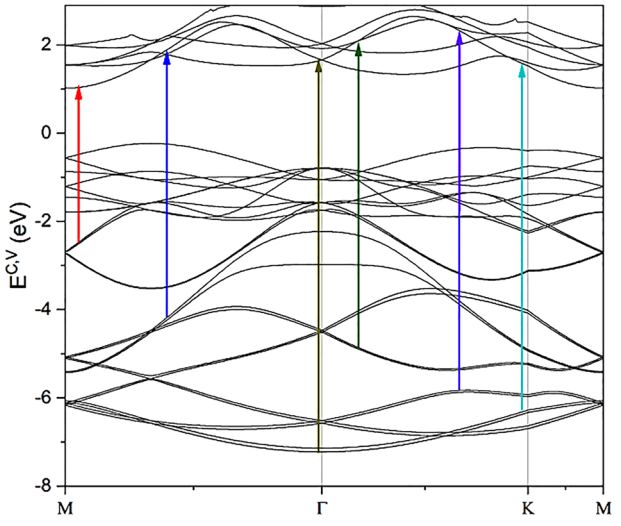

Figure 7. Interband transition of 2H-GaSe corresponding to peaks in dielectric function.

around 4.5−5.5 eV corresponding to maxima of absorption at these frequencies. The absorption band expands beyond 6 up to 10 eV in the *zz* direction associating with the transition from the valence to conduction bands. Furthermore, peaks of the energy loss function as shown in Figure 6c are consequently found in the vanished region of ε_1 for the *xx* direction. The loss function corresponds to a broadened peak at approximately 6 and 11 eV in the *xx* and *zz* directions, respectively, relating to plasmons and forms of collective excitations. The plasmon is determined by the vanishing real part of the dielectric function as mentioned above and a minimum of the imaginary part. Thus, the plasmon modes associate with the imaginary part that could propagate along the surface. Simultaneously, a small vibration is presented in increasing energy indicated in weak peaks in two parts. It should be noted that the region above 10 eV cannot be interpreted in terms of classical oscillators, which is consistent with interband transitions shown in Figure 7. In this region, ε_1 and ε_2 are dominated by linear features in which ε_1 increases while there is decreasing of ε_2. Additionally, the reflectance and refractive properties are calculated based on the dielectric function shown in Figure 6d,e. In Figure 6d, the strong reflectance minimum is determined by the imaginary part of the dielectric constant in the energy range of (0, 2) eV and (5, 6) eV for all directions and *zz*-direction, respectively, indicating a collective plasma resonance. Simultaneously, the broad maxima in (5, 6) eV and (4, 5) eV of the *xx* and *zz* directions, respectively, relate to the strong peak in the dielectric constant. Moreover, the maximum refractive index is found in low-lying energies of approximately 2.5 and 3.5 eV for two directions as described in Figure 6e. This index accordingly decreases in increasing energy with the increase of wavelength. Especially, the change in the refractive index is produced from the change of absorption through the Kramers−Kronig relationships. These two factors are consistent with characteristics of dielectric function indicating the close relation between dielectric function and linear optical properties, indicated in this relation.

https://doi.org/10.1021/acsomega.2c03198
ACS Omega 2022, 7, 34868−34876

CONCLUSIONS

In summary, the stability and electronic and optical properties of H-functionalized GaSe monolayer were investigated by implementing first-principles calculations via the VASP package. Double-site functionalization exhibits the stable structure due to formation energy and phonon dispersion. Through the band energy structure and orbital-projected DOS, a transformation of the electronic configuration was realized between two cases of functionalization corresponding to single and double sites, respectively. H-GaSe reveals a gapless structure, while semiconducting behavior was found in 2H-GaSe with a total change of band dispersion. The sp^3 bonding was exhibited based on the coexistence of s and p_z, p_y, p_z orbitals in Ga−Ga and Ga−Se, while H−Se bonds were indicated in DOS and charge density. Moreover, the band gap engineering is proposed when increasing the number L of GaSe segments for the double-site functionalization. The functionalized manner could form a different magnetic configuration as mentioned in spin density distribution. In addition, 2H-GaSe exhibits sensitive optical properties indicating the consistency of the main features through dielectric function, absorption, refractivity, reflectivity, and energy loss spectrum. This work provides useful information for the functionalization of GaSe, suggesting a validity to design this material in electronic devices.

ASSOCIATED CONTENT

Supporting Information

The Supporting Information is available free of charge at https://pubs.acs.org/doi/10.1021/acsomega.2c03198.

Calculation of relative permittivity, energy losses of fast electron, absorption, and reflectivity, plots of energy versus dielectric constant, energy loss function, absorption, reflectivity, refractive index, illustration of charge density, plot of orbital PDOS of monolayer GaSe, band energy spectrum, discussion of monolayer GaSe (PDF)

AUTHOR INFORMATION

Corresponding Authors

Ming-Fa Lin − *Department of Physics, National Cheng Kung University, East district, Tainan 701, Taiwan; Hierachical Green-Energy Materials Research Center, National Cheng Kung University, East district, Tainan 701, Taiwan;* orcid.org/0000-0002-0531-2068; Email: mflin@ncku.edu.tw

Thi My Duyen Huynh − *Department of Physics, National Cheng Kung University, East district, Tainan 701, Taiwan;* Email: huynhduyen1111@gmail.com

Author

Thi Dieu Hien Nguyen − *Department of Physics, National Cheng Kung University, East district, Tainan 701, Taiwan*

Complete contact information is available at: https://pubs.acs.org/10.1021/acsomega.2c03198

Notes

The authors declare no competing financial interest.

ACKNOWLEDGMENTS

This work was financially supported by the Hierarchical Green Energy Materials (Hi-GEM) Research Center, from The Featured Areas Research Center Program within the framework of the Higher Education Sprout Projected by the Ministry of Education (MOE), and the Ministry of Science and Technology (MOST 108-2112-M-006-016-MY3) in Taiwan.

REFERENCES

(1) Zhang, L.; Yang, Z. J. F.; Gong, T.; Pan, R. K.; Wang, H. D.; Guo, Z. A.; Zhang, H.; Fu, X. Recent advances in emerging Janus two-dimensional materials: from fundamental physics to device applications. *J. Mater. Chem. A* **2020**, *8*, 8813−8830.

(2) Rao, C. N. R.; Gopalakrishnan, K.; Maitra, U. Comparative Study of Potential Applications of Graphene, MoS2, and Other Two-Dimensional Materials in Energy Devices, Sensors, and Related Areas. *Acs Appl. Mater. Interfaces* **2015**, *7*, 7809−7832.

(3) Hussain, T.; De Sarkar, A.; Ahuja, R. Functionalization of hydrogenated graphene by polylithiated species for efficient hydrogen storage. *Int.l J. Hydrog. Energy* **2014**, *39*, 2560−2566.

(4) Sosa, A. N.; Cid, B. J.; Miranda, A.; Perez, L. A.; Salazar, F.; Trejo, A.; Cruz-Irisson, M. Light metal functionalized two-dimensional siligene for high capacity hydrogen storage: DFT study. *Int.l J. Hydrog. Energy* **2021**, *46*, 29348−29360.

(5) Cheng, Z. W.; Liu, T.; Zhao, B.; Shen, F.; Jin, H. Y.; Han, X. G. Recent advances in organic-inorganic composite solid electrolytes for all-solid-state lithium batteries. *Energy Storage Mater.* **2021**, *34*, 388−416.

(6) Novoselov, K. S.; Mishchenko, A.; Carvalho, A.; Castro Neto, A. H. 2D materials and van der Waals heterostructures. *Science* **2016**, *353*, 461−472.

(7) Manzeli, S.; Ovchinnikov, D.; Pasquier, D.; Yazyev, O. V.; Kis, A. 2D transition metal dichalcogenides. *Nat. Rev. Mater.* **2017**, *2*, 17033.

(8) Chen, J. H.; Tan, X. L.; Lin, P.; Sa, B. S.; Zhou, J.; Zhang, Y. G.; Wen, C. L.; Sun, Z. M. Comprehensive understanding of intrinsic mobility in the monolayers of III-VI group 2D materials. *Phys. Chem. Chem. Phys.* **2019**, *21*, 21898−21907.

(9) Chen, T.; Wang, L. L.; Zhang, X. H.; Luo, K. W.; Li, Q. Conductance gap induced by orbital symmetry mismatch in inhomogeneous hydrogen-terminated zigzag graphene nanoribbons. *Org. Electron.* **2015**, *26*, 181−185.

(10) Kamel, S.; El-Sakhawy, M.; Anis, B.; Tohamy, H. A. S. Graphene's Structure, Synthesis and Characterization; A brief review. *Egypt. J. Chem.* **2019**, *62*, 593−608.

(11) Lu, R. T.; Liu, J. W.; Luo, H. F.; Chikan, V.; Wu, J. Z. Graphene/GaSe-Nanosheet Hybrid: Towards High Gain and Fast Photoresponse. *Sci. Rep.* **2016**, *6*, 19161.

(12) Nguyen, M. T.; Phong, P. N.; Tuyen, N. D. Hydrogenated Graphene and Hydrogenated Silicene: Computational Insights. *ChemPhysChem* **2015**, *16*, 1733−1738.

(13) Ben Aziza, Z.; Pierucci, D.; Henck, H.; Silly, M. G.; David, C.; Yoon, M.; Sirotti, F.; Xiao, K.; Eddrief, M.; Girard, J. C.; Ouerghi, A. Tunable quasiparticle band gap in few-layer GaSe/graphene van der Waals heterostructures. *Phys.l Rev. B* **2017**, *96*, 035407.

(14) Kim, J.; Cote, L. J.; Huang, J. X. Two Dimensional Soft Material: New Faces of Graphene Oxide. *Acc. Chem. Res.* **2012**, *45*, 1356−1364.

(15) Ben Aziza, Z.; Henck, H.; Pierucci, D.; Silly, M. G.; Lhuillier, E.; Patriarche, G.; Sirotti, F.; Eddrief, M.; Ouerghi, A. van der Waals Epitaxy of GaSe/Graphene Heterostructure: Electronic and Interfacial Properties. *ACS Nano* **2016**, *10*, 9679−9686.

(16) Gao, B.; Shao, X. C.; Lv, J.; Wang, Y. C.; Ma, Y. M. Structure Prediction of Atoms Adsorbed on Two-Dimensional Layer Materials: Method and Applications. *J. Phys. Chem. C* **2015**, *119*, 20111−20118.

(17) Obodo, K. O.; Gebreyesus, G.; Ouma, C. N. M.; Obodo, J. T.; Ezeonu, S. O.; Rai, D. P.; Bouhafs, B. Controlling the electronic and optical properties of HfS2 mono-layers via lanthanide substitutional doping: a DFT plus U study. *Rsc Adv.* **2020**, *10*, 15670−15676.

(18) Iordanidou, K.; Houssa, M.; Kioseoglou, J.; Afanas'ev, V. V.; Stesmans, A.; Persson, C. Hole-Doped 2D InSe for Spintronic Applications. *Acs Appl. Nano Mater.* **2018**, *1*, 6656−6665.

(19) Wang, X.; Tian, W.; Liu, D. Q.; Zhi, C. Y.; Bando, Y.; Golberg, D. Unusual formation of alpha-Fe2O3 hexagonal nanoplatelets in N-doped sandwiched graphene chamber for high-performance lithium-ions batteries. *Nano Energy* **2013**, *2*, 257−267.
(20) Lee, H.; Bak, S.; Cho, Y.; Kim, M.; Kang, S. H.; Bui, V. Q.; Le, H. M.; Kim, S. W.; Lee, H. Hydrogen adsorption engineering by intramolecular proton transfer on 2D nanosheets. *Npg Asia Mater.* **2018**, *10*, 441−454.
(21) Nakata, Y.; Sugawara, K.; Chainani, A.; Yamauchi, K.; Nakayama, K.; Souma, S.; Chuang, P. Y.; Cheng, C. M.; Oguchi, T.; Ueno, K.; Takahashi, T.; Sato, T. Dimensionality reduction and band quantization induced by potassium intercalation in 1T-HfTe2. *Phys. Rev. Mater.* **2019**, *3*, 071001.
(22) Habenicht, C.; Simon, J.; Richter, M.; Schuster, R.; Knupfer, M.; Buchner, B. Potassium-intercalated bulk HfS2 and HfSe2: Phase stability, structure, and electronic structure. *Phys. Rev. Mater.* **2020**, *4*, 064002.
(23) Kyhl, L.; Bisson, R.; Balog, R.; Groves, M. N.; Kolsbjerg, E. L.; Cassidy, A. M.; Jørgensen, J. H.; Halkjær, S.; Miwa, J. A.; Grubisic Cabo, A.; Angot, T.; Hofmann, P.; Arman, M. A.; Urpelainen, S.; Lacovig, P.; Bignardi, L.; Bluhm, H.; Knudsen, J.; Hammer, B.ør.; Hornekaer, L. Exciting H-2 Molecules for Graphene Functionalization. *ACS Nano* **2018**, *12*, 513−520.
(24) Surya, V. J.; Iyakutti, K.; Rajarajeswari, M.; Kawazoe, Y. Functionalization of single-walled carbon nanotube with borane for hydrogen storage. *Phys. E: Low-Dimens. Syst. Nanostructures* **2009**, *41*, 1340−1346.
(25) Manjunatha, S.; Rajesh, S.; Vishnoi, P.; Rao, C. N. R. Reaction with organic halides as a general method for the covalent functionalization of nanosheets of 2D chalcogenides and related materials. *J. Mater. Res.* **2017**, *32*, 2984−2992.
(26) Handoko, A. D.; Fredrickson, K. D.; Anasori, B.; Convey, K. W.; Johnson, L. R.; Gogotsi, Y.; Vojvodic, A.; Seh, Z. W. Tuning the Basal Plane Functionalization of Two-Dimensional Metal Carbides (MXenes) To Control Hydrogen Evolution Activity. *Acs Appl. Energy Mater.* **2018**, *1*, 173−180.
(27) Almeida, R.; Banerjee, A.; Chakraborty, S.; Almeida, J.; Ahuja, R. Theoretical Evidence behind Bifunctional Catalytic Activity in Pristine and Functionalized Al2C Monolayers. *ChemPhysChem* **2018**, *19*, 148−152.
(28) Abdelkarim, O.; Kaur, J.; Liu, J. B.; Navarro-Pardo, F.; Zarrin, H.; Yurtsever, A.; Bassioni, G.; Wang, Z. M. M.; Selopal, G. S.; Rosei, F. Two-dimensional functionalized hexagonal boron nitride for quantum dot photoelectrochemical hydrogen generation. *J. Mater. Chem. A* **2020**, *8*, 20698−20713.
(29) Shen, J. F.; Wang, H.; Zhuang, P. Y.; Zeng, H. T.; Ge, Y. C.; Steven, C.; Dong, P.; Gao, S. P.; Ye, M. X. A general strategy for the functionalization of two-dimensional metal chalcogenides. *Nanoscale* **2018**, *10*, 10657−10663.
(30) Panigrahi, P.; Dhinakaran, A. K.; Naqvi, S. R.; Gollu, S. R.; Ahuja, R.; Hussain, T. Light metal decorated graphdiyne nanosheets for reversible hydrogen storage. *Nanotechnology* **2018**, *29*, 355401.
(31) Pak, S.; Lim, J.; Hong, J.; Cha, S. Enhanced Hydrogen Evolution Reaction in Surface Functionalized MoS2Monolayers. *Catalysts* **2021**, *11*, 70.
(32) Xie, J. F.; Qi, J. D.; Lei, F. C.; Xie, Y. Modulation of electronic structures in two-dimensional electrocatalysts for the hydrogen evolution reaction. *Chem. Commun.* **2020**, *56*, 11910−11930.
(33) Jiang, Y. A.; Sun, T.; Xie, X.; Jiang, W.; Li, J.; Tian, B. B.; Su, C. L. Oxygen-Functionalized Ultrathin Ti3C2Tx MXene for Enhanced Electrocatalytic Hydrogen Evolution. *ChemSusChem* **2019**, *12*, 1368−1373.
(34) Rupp, C. J.; Chakraborty, S.; Anversa, J.; Baierle, R. J.; Ahuja, R. Rationalizing the Hydrogen and Oxygen Evolution Reaction Activity of Two-Dimensional Hydrogenated Silicene and Germanene. *Acs Appl. Mater. Interfaces* **2016**, *8*, 1536−1544.
(35) Mir, S. H.; Chakraborty, S.; Jha, P. C.; Warna, J.; Soni, H.; Jha, P. K.; Ahuja, R. Two-dimensional boron: Lightest catalyst for hydrogen and oxygen evolution reaction. *Appl. Phys. Lett.* **2016**, *109*, 053903.
(36) Narvaez, W.; Priest, C.; Tang, Q.; Jiang, D. E. Hydrogen functionalisation of transition metal dichalcogenide monolayers from first principles. *Mol. Simul.* **2017**, *43*, 379−383.
(37) Wines, D.; Kropp, J. A.; Chaney, G.; Ersan, F.; Ataca, C. Electronic properties of bare and functionalized two-dimensional (2D) tellurene structures. *Phys. Chem. Chem. Phys.* **2020**, *22*, 6727−6737.
(38) Hasanian, M.; Mortazavi, B.; Ostadhossein, A.; Rabczuk, T.; van Duin, A. C. T. Hydrogenation and defect formation control the strength and ductility of MoS2 nanosheets: Reactive molecular dynamics simulation. *Extreme Mech. Lett.* **2018**, *22*, 157−164.
(39) Huang, X.; Zeng, Z. Y.; Fan, Z. X.; Liu, J. Q.; Zhang, H. Graphene-Based Electrodes. *Adv. Mater.* **2012**, *24*, 5979−6004.
(40) Yang, S. B.; Feng, X. L.; Mullen, K. Sandwich-Like, Graphene-Based Titania Nanosheets with High Surface Area for Fast Lithium Storage. *Adv. Mater.* **2011**, *23*, 3575−3579.
(41) Ratha, S.; Rout, C. S. Supercapacitor Electrodes Based on Layered Tungsten Disulfide-Reduced Graphene Oxide Hybrids Synthesized by a Facile Hydrothermal Method. *Acs Appl. Mater. Interfaces* **2013**, *5*, 11427−11433.
(42) Toh, R. J.; Sofer, Z.; Pumera, M. Catalytic properties of group 4 transition metal dichalcogenides (MX2; M = Ti, Zr, Hf; X = S, Se, Te). *J. Mater. Chem. A* **2016**, *4*, 18322−18334.
(43) Wang, Q. H.; Kalantar-Zadeh, K.; Kis, A.; Coleman, J. N.; Strano, M. S. Electronics and optoelectronics of two-dimensional transition metal dichalcogenides. *Nat. Nanotechnol.* **2012**, *7*, 699−712.
(44) Ren, C. D.; Wang, S. K.; Tian, H. Y.; Luo, Y.; Yu, J.; Xu, Y. J.; Sun, M. L. First-principles investigation on electronic properties and band alignment of group III monochalcogenides. *Sci. Rep.* **2019**, *9*, 13289.
(45) Choi, W.; Choudhary, N.; Han, G. H.; Park, J.; Akinwande, D.; Lee, Y. H. Recent development of two-dimensional transition metal dichalcogenides and their applications. *Mater. Today* **2017**, *20*, 116−130.
(46) Hu, Z. Y.; Ding, Y. C.; Hu, X. M.; Zhou, W. H.; Yu, X. C.; Zhang, S. L. Recent progress in 2D group IV-IV monochalcogenides: synthesis, properties and applications. *Nanotechnology* **2019**, *30*, 252001.
(47) Zhang, Y.; Zhang, L.; Lv, T.a.; Chu, P. K.; Huo, K. Two-Dimensional Transition Metal Chalcogenides for Alkali metal ions storage. *Chem.Sus.Chem.* **2020**, *13*, 1114−1154.
(48) Ni, Z. Y.; Minamitani, E.; Ando, Y.; Watanabe, S. The electronic structure of quasi-free-standing germanene on monolayer MX (M = Ga, In; X = S, Se, Te). *Phys. Chem. Chem. Phys.* **2015**, *17*, 19039−19044.
(49) Wang, H. M.; Qin, G. Z.; Yang, J. Y.; Qin, Z. Z.; Yao, Y. G.; Wang, Q.; Hu, M. First-principles study of electronic, optical and thermal transport properties of group III-VI monolayer MX (M = Ga, In; X = S, Se). *J. Appl. Phys.* **2019**, *125*, 245104.
(50) Antonius, G.; Qiu, D. Y.; Louie, S. G. Orbital Symmetry and the Optical Response of Single-Layer MX Monochalcogenides. *Nano Lett.* **2018**, *18*, 1925−1929.
(51) Lin, J. H.; Zhang, B. F.; Zheng, T. C. Half-Hydrogenated Monolayer Group III Monochalcogenides: Wide Direct Band Gaps and Potential Photocatalysts for Water Splitting. *J. Phys. Chem. C* **2019**, *123*, 27697−27703.
(52) Afaneh, T.; Fryer, A.; Xin, Y.; Hyde, R. H.; Kapuruge, N.; Gutierrez, H. R. Large-Area Growth and Stability of Monolayer Gallium Monochalcogenides for Optoelectronic Devices. *Acs Appl. Nano Mater.* **2020**, *3*, 7879−7887.
(53) Li, W. B.; Li, J. Piezoelectricity in two-dimensional group-III monochalcogenides. *Nano Res.* **2015**, *8*, 3796−3802.
(54) Demirci, S.; Avazli, N.; Durgun, E.; Cahangirov, S. Structural and electronic properties of monolayer group III monochalcogenides. *Phys. Rev. B* **2017**, *95*, 115409.

https://doi.org/10.1021/acsomega.2c03198
ACS Omega 2022, 7, 34868−34876

(55) Allakhverdiev, K. R.; Yetis, M. O.; Ozbek, S.; Baykara, T. K.; Salaev, E. Y. Effective nonlinear GaSe crystal. Optical properties and applications. *Laser Phys.* **2009**, *19*, 1092−1104.
(56) Huang, C. B.; Mao, M. S.; Wu, H. X.; Wang, Z. Y.; Ni, Y. B. Growth and characterization of an Al-doped GaSe crystal. *J. Cryst. Growth* **2018**, *483*, 318−322.
(57) Huang, C.-B.; WuWu, H.-X.; Ni, Y.-B.; Wang, Z.-Y.; Chen, S.-J. Optical and defect properties of S-doped and Al-doped GaSe crystals. *Chinese Phys. B* **2017**, *26*, 094211.
(58) Kim, C. D.; Jang, K. W.; Lee, Y. I. Optical properties of Tm-doped GaSe single crystals. *Solid State Commun.* **2004**, *130*, 701−704.
(59) Cao, T.; Li, Z. L.; Louie, S. G. Tunable Magnetism and Half-Metallicity in Hole-Doped Monolayer GaSe. *Phys. Rev. Lett.* **2015**, *114*, 236602.
(60) Peng, Q.; Zhou, J.; Si, C.; Sun, Z. M. Flexible quantum spin Hall insulator in O-functionalized GaSe monolayer. *J. Alloys Compd.* **2019**, *788*, 1113−1118.
(61) Hafner, J. Ab-initio simulations of materials using VASP: Density-functional theory and beyond. *J. Comput. Chem.* **2008**, *29*, 2044−2078.
(62) Perdew, J. P.; Burke, K.; Ernzerhof, M. Generalized gradient approximation made simple. *Phys. Rev. Lett.* **1996**, *77*, 3865−3868.
(63) Ernzerhof, M.; Scuseria, G. E. Assessment of the Perdew-Burke-Ernzerhof exchange-correlation functional. *J. Chem. Phys.* **1999**, *110*, 5029−5036.
(64) Heyd, J.; Scuseria, G. E. Efficient hybrid density functional calculations in solids: Assessment of the Heyd-Scuseria-Ernzerhof screened Coulomb hybrid functional. *J. Chem. Phys.* **2004**, *121*, 1187−1192.
(65) Heyd, J.; Peralta, J. E.; Scuseria, G. E.; Martin, R. L. Energy band gaps and lattice parameters evaluated with the Heyd-Scuseria-Ernzerhof screened hybrid functional. *J. Chem. Phys.* **2005**, *123*, 174101.
(66) Yanai, T.; Tew, D. P.; Handy, N. C. A new hybrid exchange-correlation functional using the Coulomb-attenuating method (CAM-B3LYP). *Chem. Phys. Lett.* **2004**, *393*, 51−57.
(67) Bahuguna, B. P.; Saini, L. K.; Sharma, R. O.; Tiwari, B. Hybrid functional calculations of electronic and thermoelectric properties of GaS, GaSe, and GaTe monolayers. *Phys. Chem. Chem. Phys.* **2018**, *20*, 28575−28582.
(68) Galashev, A. E.; Rakhmanova, O. R. Mechanical and thermal stability of graphene and graphene-based materials. *Phys-Usp* **2014**, *57*, 970−989.
(69) Seitsonen, A. P.; Saitta, A. M.; Wassmann, T.; Lazzeri, M.; Mauri, F. Structure and stability of graphene nanoribbons in oxygen, carbon dioxide, water, and ammonia. *Phys. Rev. B* **2010**, *82*, 115425.
(70) Jing, H. Increasing stability of MoS2 nanoribbons by edge engineering. *Chem. Phys.* **2021**, *548*, 111241.
(71) Jiang, W. C.; Li, B. W.; Wang, X. M.; Chen, G. Y.; Chen, T.; Xiang, Y.; Xie, W.; Dai, Y. M.; Zhu, X. Y.; Yang, H.; Sun, J.; Wen, H. H. Van Hove singularity arising from Mexican-hat-shaped inverted bands in the topological insulator Sn-doped Bi1.1Sb0.9Te2S. *Phys. Rev. B* **2020**, *101*, 121115.
(72) Zhong, C. Y.; Xie, Y. E.; Chen, Y. P.; Zhang, S. B. Coexistence of flat bands and Dirac bands in a carbon-Kagome-lattice family. *Carbon* **2016**, *99*, 65−70.
(73) Peiponen, K. E.; Vartiainen, E. M. Kramers-Kronig relations in optical-data inversion. *Phys. Rev. B* **1991**, *44*, 8301−8303.

https://doi.org/10.1021/acsomega.2c03198
ACS Omega 2022, 7, 34868−34876